WPMST1-CPR(18) 18646

A Kallenbach et al.

Neutral pressure and separatrix density related models for seed impurity divertor radiation in ASDEX Upgrade

Preprint of Paper to be submitted for publication in Proceeding of 23rd International Conference on Plasma Surface Interactions in Controlled Fusion Devices (PSI-23)

This work has been carried out within the framework of the EUROfusion Consortium and has received funding from the Euratom research and training programme 2014-2018 under grant agreement No 633053. The views and opinions expressed herein do not necessarily reflect those of the European Commission.

Neutral pressure and separatrix density related models for seed impurity divertor radiation in ASDEX Upgrade

A. Kallenbach[1], M. Bernert[1], R. Dux[1], T. Eich[1], S.S. Henderson[3], T. Pütterich[1], F. Reimold[2], V. Rohde[1], H.J. Sun[1], ASDEX Upgrade team[4], EUROfusion MST1 team[5]

[1] *Max Planck Institute for Plasma Physics, Garching, Germany,*
[2] *Max Planck Institute for Plasma Physics, Greifswald, Germany,*
[3] *CCFE Fusion Association, Culham Science Centre, Abingdon, OX14 3DB*
[4] *A. Kallenbach et al., Nucl. Fusion* **57** *(2017) 102015*
[5] *H. Meyer et al., Nucl. Fusion* **57** *(2017) 102014*

Abstract

Analytical expressions for the divertor radiation around the onset of detachment based on the divertor neutral pressure and the upstream separatrix density are tested against measurements on strongly nitrogen seeded high confinement mode (H-mode) discharges in ASDEX Upgrade. The divertor pressure is used as a key experimental parameter as far as possible, since it can be regarded as engineering parameter based on the balance of puffing and pumping. For a tentative extrapolation to future tokamak power plants, limits set by the maximum core impurity concentration via the burn conditions are related to the divertor impurity content via the divertor enrichment factor. Combined with the H-mode density limit, which is most likely a limit for the separatrix density $n_{esep}/n_{Greenwald} \leq 0.5$, estimates for the maximum separatrix power P_{sep} compliant with the achievement of detachment are presented for a density related 2-point model and a flux related radiation model. The detachment, which is assumed necessary for the achievement of sufficiently long target lifetimes, requires in H-mode the dissipation of a major fraction of the power flowing to the divertor by impurity radiation. Favorable conditions for power exhaust feature a high Greenwald density / high divertor neutral pressure. The latter also facilitates a faster helium exhaust, which increases the margin for the seed impurity concentration in the core. Major uncertainties in the extrapolation of seeded scenarios regard the divertor impurity enrichment and the power width λ in the divertor for

detached conditions.

Keywords: 52.55.Fa Tokamaks 52.40.Hf Plasma-Materials interactions, Boundary layer effects

1. Introduction

For a future tokamak power plant, like the European DEMO study [1], a minimum separatrix power flux, P_{sep}, in the range of 100-200 MW has to be present to sustain the H-mode. The radial width of the power carrying layer is expected to be of the order of a millimeter in the outer mid-plane [2]. As a consequence, a parallel mid-plane heat flux of several (about 5-10) GW/m^2 has to be attenuated to be compatible with the perpendicular heat load capability of the divertor target, which is of the order of 5-10 MW/m^2. Geometrical means, provided by a field line incident angle of about 2 degrees, yield for a standard divertor a factor of ≈ 30 reduction. Turbulent broadening of the power width in the divertor may help by a factor 2 as seen in current devices, which may further improve a bit with increasing field line length [3]. The remaining $\approx$ factor 10-20 reduction must be provided to a large extent by impurity radiative losses, since hydrogen radiation is weak at least for temperatures above 5 eV, where recombination is negligible. A high divertor electron density enhances the impurity radiation and promotes momentum losses and detachment [4]. The divertor plasma parameters consistent with power exhaust are quite in line with those required for obtaining low erosion rates of tungsten surface material. Depending on the seed impurity composition, plasma temperatures in front of the target below about 4 eV are required [5]. Due to the power flux associated with plasma recombination at the target, the ion fluxes need to be limited and thus substantial momentum loss is also required in particular in high field/high density devices. Since momentum loss mechanisms tend to become highly efficient at low electron temperature ($T_e < 3$ eV) [6], the divertor temperature reduction by seed impurity radiation can also in this perspective be regarded as a prerequisite for the solution of the power exhaust problem.

Detachment, radiative exhaust and operational limits have so far mostly been discussed on the basis of plasma parameters. These are usually no engineering parameters, but the consequence of heating and particle sources, radiation, neutral effects and transport. An important parameter for power exhaust and operational limits is the divertor neutral pressure, measured n

ASDEX Upgrade (AUG) by a baratron below the divertor roof baffle. This can be regarded as an engineering parameter, since it is to a large extent determined by the gas puff rate and the divertor pumping speed (see fig. 5 in [7]). The neutral particle flux densities, which are related to partial pressures, are also suitable parameters for the characterization of the divertor radiation when the radiative potential (total energy radiated by an injected hydrogen or impurity atom before it is lost) is considered. The neutral pressure, p_0, has also been successfully used as control parameter in ITER divertor performance simulations [8] [9]. The upstream separatrix density is another suitable parameter for a divertor radiation model. It cannot be set as directly by external actuators as the neutral pressure, but provides a close link to the H-mode density limit [10] [11].

Comparisons of simple divertor pressure and upstream density related divertor radiation models with experimental data are presented here for conditions of strong nitrogen seeding. The nitrogen radiation characteristics is similar to carbon [12], and the majority of radiation is emitted in the divertor region. With Ne [13] and Ar, no strong rise of divertor radiation could be achieved so far in AUG, since radiation from core and pedestal plays a dominant role for these species. Emphasis is put on high power and high neutral pressure conditions in AUG, since they require the smallest extrapolation step to reactor SOL conditions.

2. Outer divertor radiation

In a high power device, a major fraction of the power crossing the separatrix has to be dissipated, to avoid an outer divertor surface overload. Experimental evidence and modelling for a closed, standard divertor (vertical targets and no specific magnetic shaping) suggest that impurity divertor radiation is the key element for heat flux dissipation. Hydrogenic effects like volume recombination are important for detachment of the remaining particle/heat flux close to the target [14]. Hydrogen radiative cooling is generally weak. The e-folding width of the power carrying layer, λ, enters via its direct effect on the parallel heat flux and also its effect on the radial extension of the radiation volume. A simple but quite robust estimate of the divertor radiation in AUG is derived by spatially averaging the foil bolometer channels and multiplying it with a surface area of about 2 m^2, resulting from the poloidal length of 0.2 m times the divertor circumference of 10 m, see figure 1a. By this method, the radiation around the X-point region is not

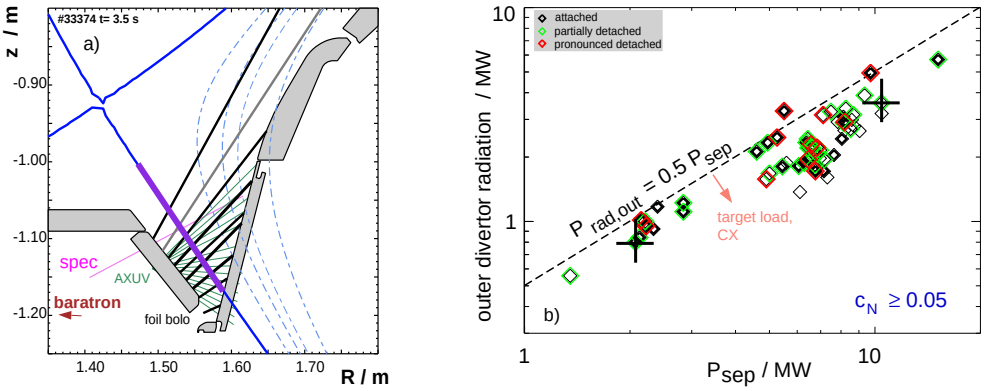

Figure 1: a) Experimental setup of the viewing lines and b) outer divertor radiation versus power crossing the separatrix, P_{sep}, for conditions dominated by seeded nitrogen, $c_N \approx \Gamma_N/7\ /(\Gamma_D + \Gamma_N/7) > 0.05$. Red colors mark pronounced, green colors partial detachment [7]. Total radiation is inferred from averaged bolometer data multiplied by a surface area of 2 m^2, see text for explanation. The crosses refer to the characteristic uncertainty in the measurements. The neutral pressure p_0 is measured by a baratron. The end of its connecting pipe at z= -1.2 m, R= 1.2 m marks its effective measurement position (indicated by an arrow, but outside view).

taken into account, as this cannot be easily separated due to contributions from the private flux and inner divertor regions to the corresponding lines of sight. Figure 1b compares the power flux crossing the separatrix, P_{sep}, with the divertor radiation measured by foil bolometers for conditions with relatively strong N seeding. P_{sep} is the difference of the absorbed heating power and the main chamber radiation derived from bolometry [15]. The measured divertor radiation close to partial as well as pronounced detachment aligns proportional to the separatrix power for a wide power range, with absolute values $P_{rad,out} \leq P_{sep}/2$. This complies with the expectation, that most of the power dispersion at detachment is provided by divertor radiation. Assuming that 2/3 of P_{sep} is directed towards the outer divertor, and that 80 % of this power is radiated at partial detachment, we expect an upper boundary of 0.53 P_{sep} to be radiated in the outer divertor. Taking into account some divertor radiation just below the X-point not accounted for by the viewing geometry, the observed range of $P_{rad,out}/P_{sep}$= 0.35 .. 0.5 complies with the expectations.

2.1. Composition of the outer divertor radiation

The radiation in the outer divertor is the most important ingredient for obtaining a sustainable power exhaust solution. Figure 2 shows time traces and analysis of nitrogen line emission and slow (0.4 ms sampling time, but effectively a few ms) calibrated foil bolometers [16] for a discharge with partial detachment by nitrogen seeding at 15 MW heating power and $c_N \approx 0.1$. Note that the total valve fluxes Γ_Z, which are injected through toroidally distributed nozzles in the roof baffle, are measured in electrons/s. Further details about pulse and spectroscopic analysis are given in [17]. The diver-

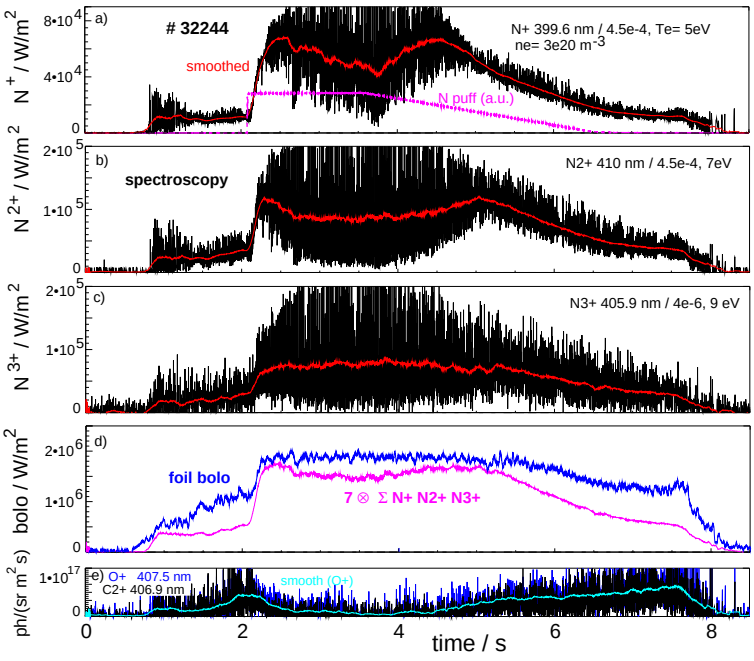

Figure 2: Divertor radiation signals taken in the middle of the outer divertor for a discharge with 15 MW heating power, $c_N \approx 0.1$ and partial detachment during the flattop phase, $I_p = 1$ MA and an ELM frequency around 150 Hz. Panels a), b), c) show spectroscopic measurements of lines emitted by N^+, N^{2+} and N^{3+}. The emitted power is plotted in terms of an extrapolated sum of all N lines of the same ionization stage, derived from ADAS96 data [18] under the assumption of electron impact excitation as dominant cause of line emission. Data for the N^+ line have been amended by Henderson [17]. The corresponding fraction of the measured line evaluated at indicated fixed T_e and $n_e = 3\ 10^{20}\ m^{-3}$ is given in the figure. Panel d) shows the total line integrated radiation from foil bolometry ch 5 (see fig. 1). Also shown is the sum of the extrapolated radiation of $N^{+,2+,3+}$ multiplied by a factor 7. Panel e) shows C^{2+} and O^+ lines, whose intensity changes opposite to the N emission.

tor radiation is strongly modulated by ELMs, as seen in the spectroscopic signals; the time resolution of the foil bolometers is too slow for temporal ELM resolution. Analysis of fast (2 μs) AXUV diodes (not shown), which exhibit a wavelength-dependent sensitivity, suggests a contribution of the ELM induced radiation to the time-averaged divertor radiation by 25-30 %. The reaction of the bolometry on the N puff occurs smoother compared to the N emission line measurements. This can be explained by the behavior of other divertor impurities (C, O, B), which show an anti-correlated emission to the N injection. The N emission seen before the start of the N puff is explained by the latency effect of a previous N seeded pulse. The slurred time behavior of the divertor radiation following N seeding and the changing contribution of other impurities suggests to consider only discharges with a dominant N divertor radiation for quantitative studies, therefore we use only conditions with $c_N > 0.05$ here. The total line integrated power emission from $N^{+,2+,3+}$ in the middle of the outer divertor fan has been extrapolated from individual emission lines around 400 nm using ADAS data. A multiplication factor of 7 is required to reach the bolometric measurement. At most a factor 2 may be expected from the omission of other ionization stages of N and molecular emission. During the seeded phase, the effect of other intrinsic impurities remains small. Hydrogenic power emission is also expected to be small. Thus, the extrapolation of the spectroscopic measurements appears a factor 3-4 too low. Substantial error contributions are expected from atomic data related to individual lines. Henderson [17] provided improved data for N^+ which resulted in a factor 2 higher radiated power from the N^+ species. Improvements for $N^{2+,3+}$ are not yet available. It should also be noted that better agreement of the extrapolated power with the bolometry can be obtained when a lower T_e is used. The total emission fraction factors shown in figure 2 decrease by about a factor 2 when the assumed electron temperatures are reduced by 2 eV with respect to the T_e values given in the figure. These estimates reveal substantial uncertainties regarding a quantitative understanding of the divertor radiated power, related to atomic data as well as to plasma parameters.

2.2. Radiative loss function and radiative potential

Divertor impurity radiation can be described by the radiative loss function, L_z, with the local radiated power density, $P_{cool} = c_z\ n_e^2\ L_z$ [19]. n_e is the local electron density and c_z the impurity concentration. For typical divertor conditions, L_z depends on a non-coronal parameter expressed as $n_e\tau_z$,

where τ_z is the impurity residence time in the divertor volume and n_e scales the inverse characteristic time for atomic physics. Alternatively, the global divertor radiation is related to the particle influx via the radiative potential [20], $\Phi_z = \tau_z\ n_e\ L_z$. The radiative potential is understood as the energy which is radiated by an impurity atom during its residence time after entering the divertor plasma. The total radiated power can be expressed as $P_{rad,div} = \Gamma_{z,dp}$ A e Φ_z, where $\Gamma_{z,dp}$ is the impurity flux density towards the divertor plasma and A the receiving surface area. Figure 3 shows L_z and Φ_z for N and Ar for 2 different values of the non-coronal parameter $n_e\tau$. Each radiation model

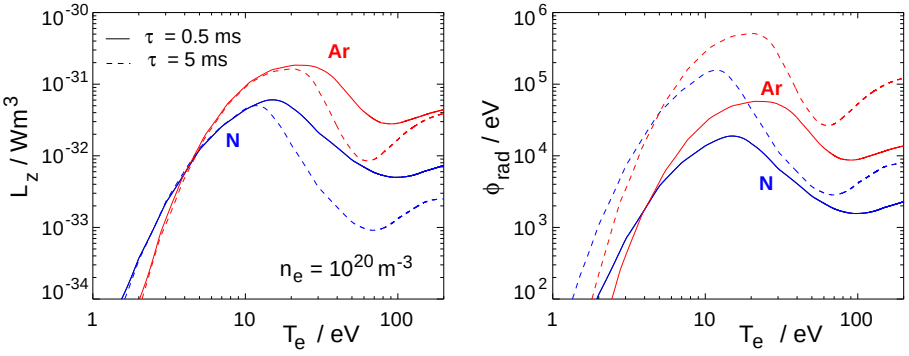

Figure 3: Radiative loss function L_z and radiative potential Φ_z for N and Ar and 2 values of the non-coronal parameter $n_e\tau_z$ [18].

is best matched to the experimental situation for conditions where its dependence of the non-coronal parameter is weak. This applies to L_z for T_e below 10 eV and above 200 eV (for Ar) and to Φ_z for the intermediate range ($\approx$ 20 -100 eV for N). The question about the better suited model is also related to the availability of experimental data. E.g., the divertor impurity concentration c_z is usually not known, while fluxes are more often available. The use of L_z has the advantage that an analytic integral [19] can be used to get an expression of the maximum radiated power, which takes into account the change of n_e and T_e along the field line assuming Spitzer conductivity and pressure balance [6].

2.3. Flux related model for divertor radiation at the onset of detachment

The most important parameter for any divertor radiation model is the impurity concentration c_z, which is generally not measured in the divertor. Reasons are lack of atomic data in sufficient quality and strong variations of

plasma parameters along viewing lines [17]. It has been found suitable, from the perspective of the comparison of divertor radiation with simple 2-point models, to use the fractional impurity atomic influx, $F_{valve,z}$ taken from the gas valves instead, resulting for nitrogen in $c_N = F_{valve,N}/7/(F_{valve,D}+F_{valve,N}/7)$ [21]. The factor 7 comes from the definition of AUG valve fluxes in terms of electrons/s. This definition neglects possible wall sticking/release and assumes equal pumping speeds for N and D. In case of N seeding, formation of ammonia [22] and wall sticking may strongly affect the particle balance. Therefore experimental conditions with steady state conditions are aspired, where formation and release largely balance. Under these conditions, agreement within 30 % between c_N from the valve flux ratio and the spectroscopic analysis is achieved [23]. Substantial D puffing is also a prerequisite for the reduction of the influence of wall D capture and release [24]. The used definition of the impurity concentration is better suited to a flux related model for divertor radiation, since the ion distribution in the divertor plasma may differ from the source ratio.

An empirical model for divertor dissipation at the onset of detachment [25], which has been corroborated by 1D modelling [21] relates the onset of detachment for a given separatrix power to the deuterium and impurity partial neutral pressure. To express P_{sep} at detachment in terms of outer divertor radiation, we assume again $P_{rad,outerdiv,det} = 0.53\ P_{sep}$. The obtained equation 1 for the divertor radiated power agrees within a factor of two with the measured divertor radiation around the onset of detachment, as shown in fig. 4.

$$P_{raddiv,out,det} = \ 4.1 \cdot 10^5\ p_0\ R\ (1 + c_z f_z)\ [W, Pa, m] \qquad (1)$$

p_0 is the neutral sub-divertor pressure in Pa, R the major radius and f_z a weighting factor for the corresponding impurity radiation capability derived from 1D modelling of detachment onset using atomic data from ADAS [21]. For (N, Ne, Ar) values f_z = (18, 45, 90) were obtained, which can be interpreted as relative radiation potentials. P_0 is measured by a baratron in the lower high field side region below the divertor roof baffle [7]. p_0 represents the flux density in the lower divertor region, but spatial variations up to about 30 % are observed depending on the extent of the high field side high density situated above the X-point on the HFS, as observed in AUG and JET [26].

It should be noted that the D pressure related part in eq. 1 is connected both to D radiation and to the increase of n_e with D pressure, which leads

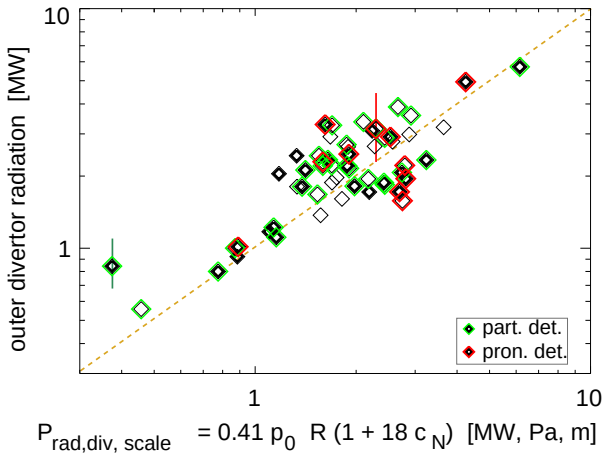

Figure 4: Measured divertor radiation flux/pressure based scaling, equation 1. The scaling corresponds to the energy loss by an N atom entering the divertor plasma of 5 keV (radiative potential around T_e= 30 eV, see figure 3b), with an effective flux receiving area of $2\pi R\lambda_{flux} \approx 0.15$ m^2.

to enhanced impurity radiation at given c_z. The use of the sum of weighted pressures has also been obtained from considerations of the global energy balance in a recent review on divertor detachment [14].

The impurity related divertor radiation according to the empirical scaling eq. 1 can be compared to the expression obtained using the radiative potential:

$$P_{raddiv,out,z} = F_z\Phi_z = 1.5\ 10^{23}\ c_z\ p_0\ 2\pi R\ \lambda_{flux}\ e\Phi_z[W,\ Pa,\ m,\ m, eV] \quad (2)$$

Assuming flux balance, the measured pressure (room temperature at baratron location) [7] can be related to a flux density Γ_0= 1.5 10^{23} at/(m^{2}s) $\cdot$ p_0/Pa in the outer divertor. $2\pi R\lambda_{flux}$ is the flux receiving area. Taking the radiative potential Φ_N = 5 keV as a typical value from fig. 3b, the perpendicular flux receiving length λ_{flux} is obtained by setting equal eq. 2 and the measured, N dominated divertor radiation. An effective length $\lambda_{flux} \approx$ 1.5 cm is obtained, which corresponds roughly to the power footprint along the target. We conclude that the impurity radiation part can be reasonably described by the ansatz of the radiative potential.

2.4. Density related radiation model

Goldston [10] has more elaborate 2-point model based analytical scalings [19] [6] for the maximum separatrix power P_{sep} which can be exhausted by

divertor radiation. The 2-point model has been extended by a prediction of the power width λ following a heuristic drift model [27].

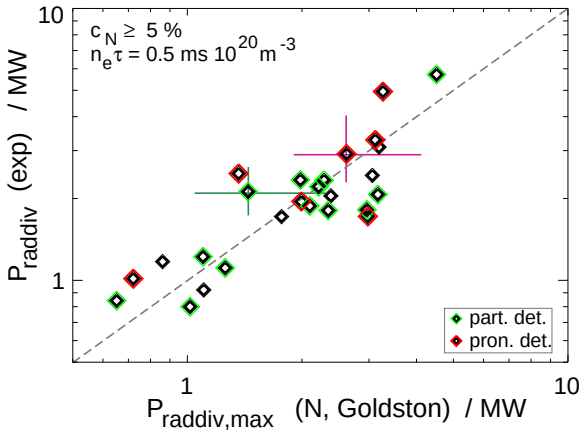

Figure 5: Measured outer divertor radiation in AUG against the predicted maximum divertor radiation according to the scaling by Goldston [10]. $n_{e,sep}$ and $T_{e,sep}$ are taken from Thomson scattering, c_z from the N/(D+N) valve flux ratio. Data are a subset of those shown in figure 4 with available $n_{e,sep}$ measurement. $n_{e,sep}$ variation is 1.5 - 4.7 10^{19} m^{-3}, $n_{e,sep}/n_{GW}$= 0.15 - 0.4.

We use the simple c_N estimate based on relative valve fluxes described in section 2.3. The maximum upstream parallel heat flux which can be radiated by N has been evaluated following [10] to

$$q_{\parallel,maxrad} = c_{rad,N} \cdot \frac{n_{e,sep}}{10^{20}\ m^{-3}} \cdot \left(\frac{T_{e,sep}}{150\ eV}\right)^{1.5} \cdot (c_N \kappa_z)^{0.5} \qquad (3)$$

with fixed non-coronal parameter. κ_z is the finite-Z correction of the electron parallel conductivity. c_{rad} corresponds to the square root in eq. (1) in [10], divided by $\sqrt{T_{e,sep}}$. By this, the temperature dependence of the atomic data has been factored out to obtain the simple expression eq. 3. c_{rad} is calculated from ADAS data for n_e= 10^{20} m^{-3} and a residence time τ= 0.5 ms, resulting in $c_{rad,N}$= 3.7 GW/m^2. Corresponding values for Ne and Ar are $c_{rad,Ne}$= 7.2 GW/m^2 and $c_{rad,Ar}$= 8.5 GW/m^2. The corresponding maximum divertor radiation is

$$P_{rad,div,max} = q_{\parallel,maxrad}\ 2\pi R f_{broad}\ < \lambda_{q,HD} >< B_p > /B \qquad (4)$$

Following [10] the broadening factor f_{broad} takes into account the Gaussian broadening of the heat flux layer in the divertor by an assumed factor b=1.79

and the effect of the broadening of the radiative layer w.r.t. the power flux, which enters as factor 1.27, leading to f_{broad}= 2.27. Using Goldston's model, poloidally averaged values $< \lambda_{q,HD} >$ and $<B_p> = \mu_0 I_p / (2\pi a\sqrt{(1+\kappa^2)/2})$ are used. $< \lambda_{q,HD} >$ is about a factor 2 larger than $\lambda_{q,omp}$ obtained from the experimental Eich scaling for the outer mid-plane and unseeded conditions, which matches AUG IR measurements [2] and also $\lambda_{Te}/3.5$ following Spitzer conductivity within 30 % [7]. The factor 2 is largely reconciled by the variation of averaged vs. omp flux expansion, $B_{p,omp}(R+a)/(<B_p>R) \approx 1.8$. In slight variation of Goldston's model, a correction factor of 0.5 has been applied to c_z in formula 10 for the Z_{eff} correction of the parallel thermal conductivity in [10] to take into account an expected decrease of c_z towards the mid-plane (high N enrichment, see sec. 3.2). This measure reduces $\lambda_{q,HD}$ and the predicted radiation by up to 10% at high seeding level [2]. In case no experimental $T_{e,sep}$ is available, it is calculated with the 2-point model ansatz

$$T_{e,sep} = (\frac{7}{2} q_{\parallel} \pi q_{cyl} R/(\kappa_z \kappa_0))^{2/7} \quad (5)$$

If this $T_{e,sep}$ is used in combination with equations 3 and 4 to calculate the maximum divertor radiated power, the finite Z correction κ_z almost cancels out.

The agreement of the predicted maximum radiation and the bolometric measurements within about +50/-30 % shown in figure 5 is surprisingly good, since one has to consider several simplifications in the radiation model: omission of D radiation and CX, the effect of ELMs, assumption of constant c_z along the field line, fixed divertor broadening leading to $1.79\lambda_q$, effects of $T_i > T_e$. The emission of intrinsic impurities (B, C) adds to the measured divertor radiation. It should be noted that this radiation model calculates the total SOL radiation including the region above the X-point, which is not included in the measurement. On the other hand, the impact of the radiation from the main SOL is small since most of the radiation is expected to be concentrated in the divertor, due to the high density and high values of L_z. Equation 4 predicts the maximum possible radiated power in the outer divertor. Therefore it should be compared to highly radiating discharges close to detachment. This condition is approximately fulfilled for the green and red data points in figure 5 since they have detached strike points, the other points are expected close by since only data with $c_N > 0.05$ are used. The radiation model used here does not contain any fitting parameter. However, it should be mentioned that the choice of the non-coronal parameter $n_e\tau_z$

dates back on a comparison of divertor radiation and bolometric measurements in AUG [21]. It is also consistent with SOLPS calculations for N and Ne. Nevertheless, an independent determination of $n_e\tau_z$ ideally as a local divertor parameter is beneficial. E.g., reduction of τ_z to 0.1 msec would lead to an increase of c_{rad} by 70 % for N and about 40 % for Ne and Ar.

3. Limits to radiative divertor cooling

There are several limitations to the impurity level or required divertor density / neutral pressure in particular for a burning device. Impurity seeding for divertor cooling does not usually cause confinement degradation in present devices, sometimes even an improvement is observed [28]. This has been related to a reduction of the high field side high density by seed impurity radiation in AUG, leading to an inward shift of the density profile, reduced $n_{e,sep}$ and improved edge stability [28]. An improvement of pedestal stability and confinement has also in JET been related to an inward shift of the density profile. The origin of the shift, and a possible relation to a high field side high density region, remained so far unclear [29].

To satisfy the necessary exhaust conditions, a high separatrix density / divertor neutral pressure may be indispensable. The question whether sufficient energy confinement can be achieved simultaneously is out of the scope of the present study. In the following, we briefly address the H-mode density limit, the maximum impurity concentration and the effect of radiation concentration around the X-point.

3.1. H-mode density limit

Following the L_z based radiation model, power exhaust improves with the upstream separatrix density, $n_{e,sep}$. This parameter is limited by the H-L density limit (HDL), which was recently explained by the combination of a fixed gradient length relation for electron pressure and power, L_p / L_q= 2, which allowed to relate the pressure gradient to the well-established Eich scaling for the power width and the ballooning stability limit. The HDL was found to occur at $n_{e,sep,HDL} \approx n_{GW}/2$ [11], with the Greenwald density $n_{GW}= 10^{14}\ I_p/\ (\pi a^2)$. The HDL thus limits the maximum divertor radiation [10] and comes in addition to the H-L power limit, which is associated with a minimum separatrix heat flux required to sustain the H-mode [30]. Margins towards moderately higher $n_{e,sep}$ values can be expected from increasing the MHD limits by shaping and density profile tailoring by pellets. A very weak

negative total P_{sep} dependence [11] may reduce the maximum $n_{s,sep}$ values at very high separatrix power.

3.2. Maximum permitted core impurity concentration and divertor enrichment

Core energy balance criteria limit the maximum permitted impurity core concentration. Seed impurities mainly used for divertor cooling (N, Ar) act in particular via fuel dilution. Pütterich et al. [31] calculated the 0D power balance including several radiative losses and the effect of fuel dilution, taking the normalized He residence time τ^*_{He}/τ_E as parameter. The latter depends on the He divertor enrichment, the neutral D divertor pressure and the pumping speed. We evaluate maximum burn-compatible core concentration of either c_N^{max}= 0.03, c_{Ne}^{max}= 0.018 or c_{Ar}^{max}= 0.006 for τ^*_{He}/τ_E =5. The latter corresponds to a He core concentration of about c_{He}= 0.08, a lower core He concentration would allow a higher seed impurity level. The maximum values given above describe the limits where burn can be sustained, for realistic and economical more feasible conditions, we assume one half of the maximum concentrations to be acceptable in the core plasma, where possible some additional high-Z radiator has to be considered.

The parameter which allows the connection of divertor and core parameters and limits is the impurity divertor enrichment, defined here using the ratio of the valve fluxes as proxy for c_z, E= $\frac{F_{valve,Z}/Z}{F_{valve,D}+F_{valve,Z}/Z}/\frac{n_{Z,core}}{n_e}$. Experimental data on enrichment in a closed divertor geometry are scarce. He has a very low enrichment value around E=0.5 [32], so in fact a de-enrichment occurs. Larger enrichment is expected for the heavier noble gases used as seed impurities [33]. A major parameter determining the enrichment is the ionization length, compared to that of D. The impurity charge enters also via effects of drifts and thermal forces. The main reason for the low enrichment of He is its ionization 'behind' the D ionization front, which means that He is not entrained in the strong D flow towards the target. This is not the case for the divertor seed impurities N and Ar. High enrichment values for N with values for E above 10 during pellet injection have been observed in AUG [34]. Ar values are expected in the same order of magnitude, but have not been measured yet. Lower enrichment values compared to N are seen for Ne, which has a higher ionization energy and a longer neutral mean free path compared to N and Ar. The above mentioned ordering is also in line with direct measurements during puff and pump experiments with an open divertor on DIII-D [35]. In the following estimates, we use E= 10 for N and

Ar. Such a high value seems realistic, since pellet injection is foreseen for the fueling of a burning device. In addition, a higher pedestal temperature will reduce the neoclassical peaking of impurities from the separatrix towards the pedestal top [36]. The low enrichment of He requires a relatively high pumping speed for keeping the core He concentration sufficiently low. In case of strong divertor radiative cooling this is then inevitably connected to a high fuel and seed impurity throughput.

3.3. X-point radiator

With proceeding (i.e. pronounced [25]) detachment, a localized radiation zone on closed field lines in the X-point region develops in several tokamaks, including AUG and JET [37] [13] [38]. The presence of the X-point radiator is accompanied by a reduction of the pedestal top temperature and a rise in density. Overall, a moderate confinement reduction is observed, where a pedestal top pressure degradation is partly compensated by a steeper gradient further inside. ELM sizes are considerably reduced, which may offer an attractive use for X-point radiator scenario for ITER and DEMO. However, since modelling is not yet advanced enough for an extrapolation, in particular regarding energy confinement, the occurrence of the X-point radiator can be regarded as an operational limit for a seeded scenario. Stable control of the radiation zone within the outer divertor leg may help to optimize the divertor radiating regime [39] towards a higher upstream radiation level.

4. Extrapolation and scaling relations

For an extrapolation of the scaling relations for the divertor radiation to devices with larger size and field, it is instructive to follow both the density and the flux related scalings. For AUG parameters both scalings deliver similar predictions, which has been reconciled by 1D modelling [21]. The connecting element is the relation of recycling flux, on the one hand, and electron and impurity density, on the other hand. Regarding extrapolation, the density related (Goldston) model is better suited due to its inclusion of a realistic n_e, T_e variation along the flux tube given by pressure balance and Spitzer conductivity. A problem of extrapolation is caused by the non-Coronal conditions, which are expected to deviate from the AUG parameters when extrapolated to high $n_{e,sep}$ values. At higher $n_{e,sep}$, the divertor density is expected to rise, and the impurity recycling flux R_z will increase at least with the square of the density according to the high-recycling 2-point model.

Consequently, the impurity residence time $\tau_z \propto c_z\ n_e/R_Z$ will decrease, and L_z rises due to the rising non-coronal contribution. Therefore, the density related model leads to a moderate (less than by the square root of the relative $n_{e,sep}$ variation) underestimation of the divertor radiation when $n_{e,sep}$ is increased and $n_e\ \tau_z$ kept constant. In contrast, the flux based scaling is expected to overestimate the divertor radiation for this parameter variation due to the reduction of $n_e\ \tau_z$ with rising $n_{e,sep}$ (recall that $\Phi_z = \tau_z\ n_e\ L_z$). The increase of L_z due to the non-Coronal contribution reduces the effect of the decreasing $n_e\ \tau_z$, but a net decrease of Φ_z is expected to remain. Dedicated scans with validated 2-D modelling are required to obtain more quantitative predictions for the increase of the divertor radiation with $n_{e,sep}$.

4.1. Relation of divertor neutral pressure and upstream separatrix density

For extrapolation with the flux based scaling, one needs to establish the relation between $n_{e,sep}$ and the D recycling flux. A direct regression of these quantities led to the relation $n_{e,sep} \propto p_0^{0.31}$ for N seeded and non seeded ASDEX Upgrade H-mode conditions, with litte impact of other parameters [7]. Such a fit is not suitable for extrapolation to other machine sizes and power levels, therefore a refined two-point model has to be used to reveal e.g. the size dependence. It should be noted that the underlying assumption of pressure balance between divertor and midplane [40] is assumed to be quite independent from divertor geometry, while the assumptions on the neutrals require a closed divertor and may depend also on divertor geometry.

The relation between the upstream density $n_{e,sep}$ and the perpendicular target ion flux density, neglecting convection, can be written as [7] [41].

$$n_{e,sep} = \frac{(1-f_{pow})^{1/2}}{1-f_{mom-loss}}\ \frac{2}{e}\left(\frac{2\kappa_0\kappa_z}{7\pi q_{cyl}R}\right)^{2/7}\ (m_D/2)^{0.5}\ q_{\parallel,mid}^{3/14}\ (\Gamma_{i,\perp}/(b\ \gamma \sin(\alpha)))^{1/2} \tag{6}$$

To obtain a relation to the neutral pressure, we assume the target ion flux to be equal to the neutral flux towards the outer divertor plasma. The flux densities are assumed equal to the flux densities obtained from the baratron measurement below the divertor [7]. At the baratron location, the neutral flux can be related to room temperature thermalized molecules, leading to $\Gamma_0 = 1.5\ 10^{23}\ \mathrm{at/(m^2 s)} \cdot p_0/\mathrm{Pa}$. This assumes a free streaming of neutrals, thus neglecting neutral-neutral collisions and no strong net particle flows between outer and inner divertor.

The unknown factors for power loss, momentum loss and divertor broadening in equation 6 were merged into a combined expression, where also a correction factor f_{0geo} has been introduced which takes into account possible variations caused by using the sub-divertor p_0 instead of the outer divertor Γ_i. The expression is expected to be of the order of 1, which is the limit for absence of any losses, divertor broadening and geometrical correction. Inserting the parallel heat flux and the other parameters from the AUG experimental database, the unknown combination of momentum loss factor, power loss factor and divertor heat flux broadening factor b is found by regression analysis to depend mainly on the neutral pressure p_0:

$$\frac{(1-f_{pow})^{1/2}}{1-f_{mom-loss}} b^{-1/2} f_{0geo} \approx c_{pres}\ p_0^{-1/4} \tag{7}$$

with c_{pres}= 0.35 [$Pa^{1/4}$]. Expressing $q_{\parallel,mid}$ via $\frac{2}{3}$ P_{sep} divided by λ_q, the circumference and the magnetic pitch factor, we finally obtain the relation of mid-plane density and divertor recycling for the considered AUG conditions around partial divertor detachment

$$n_{e,sep} = \ c_{pres}\ \frac{2}{e}(\frac{2\kappa_0\kappa_z}{7\pi q_{cyl}})^{2/7}\ (\frac{m_D}{2})^{0.5}\ R^{-0.5}\ (\frac{P_{sep}B}{3\pi < \lambda_{q,HD} >< B_p >})^{3/14} \tag{8}$$
$$\cdot(\gamma \sin(\alpha))^{-1/2}\ (1.5\ 10^{23} Pa/(at\ m^{-2}s^{-1}))^{0.5}\ p_0^{1/4}$$

We see that the partial cancelling of $p_0^{0.5}$ from the 2-point model and $p_0^{0.25}$ from the loss factor fit is critical. Therefore, eq. 8 is still limited in use for extrapolation, but it describes the relation of p_0 and $n_{e,sep}$ with 20 % rmse in $n_{e,sep}$ within the AUG parameter range. Deviations are expected e.g. due to neutral-neutral collisions at higher p_0. Note also that the factor $R^{0.5}$ provides a positive extrapolation to large devices regarding divertor recycling. Physically, this factor results from the reduction of $n_{e,sep}$ due to the increase of $T_{e,sep}$ with connection length, at constant electron pressure, and from the smaller $q_{\parallel,mid}$ at given P_{sep} in a device with larger major radius.

Figure 6 shows measured separatrix densities versus the neutral pressure as well as corresponding SOLPS calculations. The SOLPS calculations have been performed for a D gas scan (N only as trace impurity) under conditions typical for the experimental database, I_p= 0.8 MA. The relation of $n_{e,sep}$ and the neutral pressure below the roof baffle is found in the range $n_{e,sep} \propto p_0^{0.255\ ...\ 0.275}$ [42], depending on grid boundary conditions, and qualitatively consistent with eq. 8.

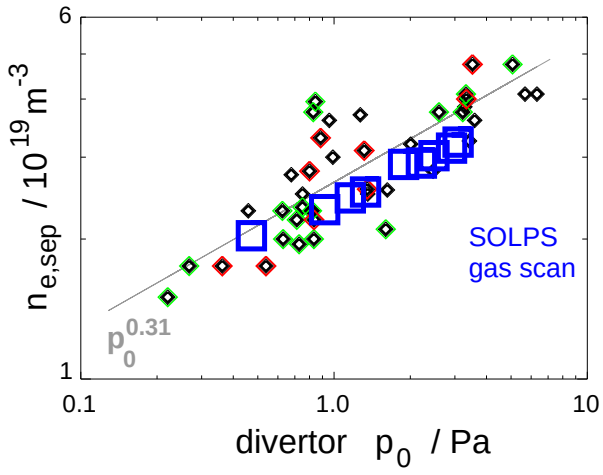

Figure 6: Measured separatrix densities versus the neutral pressure. The direct fit [7] is also indicated. Results of a SOLPS gas scan in a typical parameter range of the experimental data are shown as blues squares.

4.2. Parameter variations

The successful benchmark of the density-based and pressure-based models for divertor radiation at the onset of detachment in AUG motivates an extrapolation to possible future device parameters. Some obstacles arise for the two models in particular for high field / high density devices. A major uncertainty for both models lies in the non-coronal parameter $n_e\tau_z$. The flux related model suffers in particular from an uncertain extrapolation of the recycling flux.

Figure 7 shows extrapolated values of the maximum separatrix power compatible with detached divertor operation based on the scalings described in sections 2.3 and 2.4. Fixed, maximum divertor impurity concentrations c_N^{feas}= 0.15 and c_{Ar}^{feas}= 0.03 were used, corresponding to half the values allowed from the burn conditions [31] under the assumption of a divertor enrichment E=10 for both for N and Ar. $n_{e,sep}$ has been fixed to $n_{GW}/2$. The maximum outer divertor radiation is then calculated using the atomic data shown in figure 3 for fixed $\tau_z n_e$= 0.5 ms 10^{20} m^{-3}, and P_{sep} = $P_{rad,div,out}$ / 0.53. An iterative scheme is used to obtain self-consistent values of P_{sep}, $T_{e,sep}$ from eq. 5 and the power width $< \lambda_{q,HD} >$ (from eq. 5 in [10]), as well as for the calculation of p_0 from eq. 8.

Figure 7a shows an arbitrary field scan at constant size, starting at AUG parameters and increasing $I_p \propto B_t$ up to a factor 5 at constant geometry

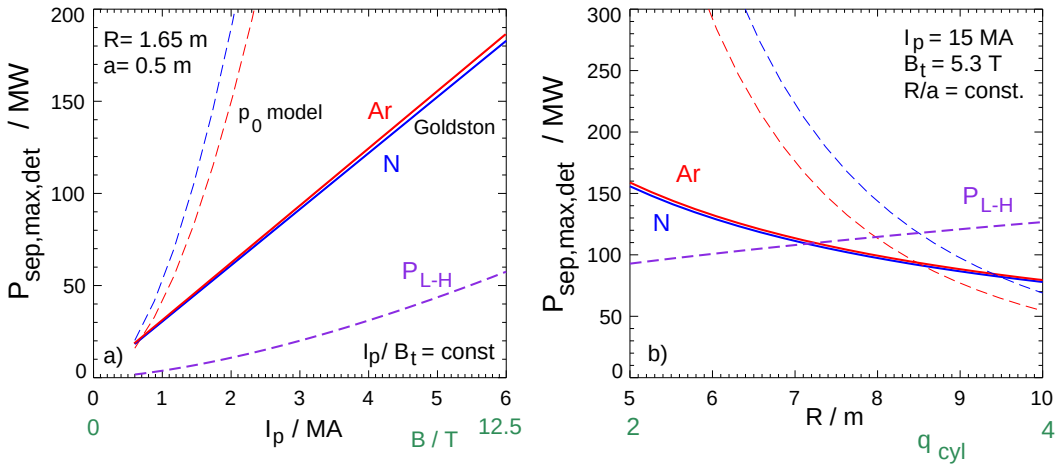

Figure 7: Extrapolated max. separatrix power for detached conditions for two machine class scans: a) B_t/I_p scan at fixed size, starting at AUG parameters at q_{95}= 3.7 / q_{cyl}= 3.1, and b) size scan at constant R/a, B_t = 5.3 T, I_p= 15 MA. ITER point at R= 6.2 m. $n_{e,sep}$ = 0.5 n_{GW}. Dashed lines are based on the flux related model, straight lines on the density related model. As a consequence of the assumptions made on $n_e\tau_z$, the actual value is expected in between the dashed and solid lines. Due to I_p kept constant, q_{cyl} rises with R, n_{GW} decreases $\propto 1/a^2$ from 1.8 10^{20} to 4.6 10^{19} m^{-3}. ITER parameters are met at R= 6.2 m. P_{sep} is assumed to be 1.875 times the corresponding maximum divertor radiation levels. The L-H power threshold [30] has been evaluated for $\overline{n}_e$= n_{GW}. Divertor seed impurity concentrations c_N= 0.15, c_{Ar}= 0.03. $n_e\tau_z$= 0.5 ms 10^{20} m^{-3}.

and q_{cyl}= 3. A fixed n_e τ_z value has been used in the calculation. Since the expected trend for decreasing n_e τ_z with increasing $n_{e,sep}$ leads to an increase of the extrapolated divertor radiation for the density related model and to a decrease for the flux based model, the expected value should lie in between the corresponding curves.

Figure 7b shows a size scan for fixed toroidal field B_t= 5.3 T, and I_p= 15 MA. Elongation, safety factor and minor radius were changed slightly compared to fig. 7a in order to match I_p = 15 MA for the ITER size R=6.2 m. For this parameter choice, the safety factor rises $\propto$ R and n_{GW} decreases quadratically $\propto 1/a^2$. At large size and elevated q_{cyl}, this scenario corresponds to an extreme case of a steady state tokamak. For the conditions of figure 7b, $n_{e,sep}$ and neutral pressure are in the same ballpark as the data from AUG, making the extrapolation more reliable compared to the B scan. In a scan similar to b) (not shown), the plasma current was increased $\propto$ a in a size scan. Thus, q_{cyl} is kept constant and n_{GW} decreases $\propto 1/a$. For these

conditions, starting at ITER values, the maximum P_{sep} from the Goldston model stays constant around 130 MW, the flux based model is a factor 2 higher and slightly decreasing.

The density related / Goldston model follows the scaling given in [10], $c_{z,det} \propto P_{sep,max,det} /(< B_{pol} > (n_{e,sep}/n_{GW})^2)$. Both models also support the conclusion in [43] that maximum toroidal field and minimizing device size maximizes the feasibility of reaching detachment. Quite unfavorable exhaust conditions are predicted for large devices with low plasma current and Greenwald density, as shown in figure 7b.

Quite similar values for the maximum detachable P_{sep} are obtained for N and Ar since the effects of different radiative capabilities and allowed concentrations cancel. Not very favorable divertor cooling scenarios have been obtained so far with Ne both in AUG and JET [13], accompanied also by an impact on the pedestal profiles. Suspected reasons are a lower divertor enrichment or the low radiative loss power of Ne at low T_e. If we assume the enrichment to be the factor 2.2 lower for Ne compared to N and Ar, its curves lie very close to those of N and Ar. On Alcator C-Mod, higher divertor radiation levels were also obtained with N compared to Ne and Ar [44].

When judging the results of figure 7, it should be kept in mind that the density based model has a more accurate physics basis due to the consideration of n_e and T_e variations along the field line. The flux based model has the advantage of better availability of experimental input parameters. The divertor neutral pressure / flux based model should not be used for far extrapolation, since the ansatz $P_{sep} \propto p_0\ (1+c_z f_z)$ is a fit function and not directly connected to a physics model. Beyond p_0= 10 Pa, the mean free path of neutrals becomes smaller and fluxes are expected to be impeded, and eq. 8, which is a fit to experimental data for AUG conditions, is no longer valid.

The prediction for a large device with moderate plasma current are quite pessimistic due to its low Greenwald density and hence low $n_{e,sep}$ and neutral pressure. Therefore an alternative divertor configuration may be required for such a device. For ITER operation with half current and field, the expected lower maximum separatrix density and hence neutral divertor pressure is expected to result in a reduced power exhaust capability, which is however compatible with the reduced heating power. Regarding local divertor parameters, the extrapolation is within the range of divertor conditions in AUG H-mode plasmas. The largest uncertainties concern for the density re-

lated model the divertor power width in a high current device and for the flux based model effects of divertor geometry. In present day devices, the wish to operate at low core density/collisionality e.g. for the achievement of high current drive fractions is not compatible with the high $n_{e,sep}$ or high divertor neutral pressure needed for the exhaust of high power. For reactor size machines, core and edge densities are expected to be decoupled due to the SOL opacity for neutrals and predominant pellet fueling.

Generally, a high plasma current density is favorable for power exhaust, if the possibility of using a high separatrix density or divertor neutral pressure is fully exploited. To strengthen the predicted operational parameter point, an improved version of the current H-L power scaling is desirable, which includes radiation losses and takes into account the separatrix/pedestal density.

To strengthen predictions for high neutral divertor pressure, experimental data in this parameter range are required. Currently, high pressure operation at high P_{sep} is limited in AUG by NBI tripping due to beam blocking in the duct, which so far occurred for divertor pressures around 7 Pa. Stable operation near the H-mode density limit is thus so far only possible up to I_p= 0.8 MA, or correspondingly $n_{e,sep}$ <5 10^{19} m^{-3}.

5. Conclusions

Two different simple analytical predictions for divertor radiation and radiative cooling are able to describe within a factor 2 the outer divertor radiation for conditions of strong N seeding in AUG. The analytical models are expected to hold for Ar as well, which is considered as a combined core and divertor radiator for large devices [45] [46]. The most important uncertainties are the power width in the divertor for low temperatures and the impurity enrichment in the divertor in relation to the plasma core. The limitation of the upstream separatrix density by the H-L transition [11], or the corresponding limitation of divertor neutral pressure [7], appear as key restrictions for the achievable maximum divertor radiation.

The neutral pressure measured at the bottom of the divertor (see fig. 1), p_0, is an engineering parameter which is closely connected to tokamak operational conditions and limits. Reduced physics model allow to establish its relation to divertor detachment and the H-L density limit. The maximum neutral pressure compatible with H-mode operation, given by the relation of p_0 and $n_{esep,max}$, set the limit for the maximum P_{sep} where detachment can be achieved when the maximum impurity concentration is given by the burn

condition and the divertor enrichment both for the seed impurity and He. 2D modelling, well calibrated against experimental parameter scans, is required to solidify the assumed relation of $n_{e,sep}$ and p_0 and to calculate absolute values of the divertor impurity enrichment. For the latter, the impact of small ELMs or the ELM-preventing instability has to be taken into account.

The behavior of the divertor heat flux broadening for detached conditions at the strike point is not well known, since high precision IR measurements of the heat flux profile are not applicable under such conditions. Also, in a large DEMO-type device, broadening mechanisms leading to a larger $\lambda_{q,div}$ may become effective [3], which are not easily measured with current short connection lengths. Validation of the radiative losses are hampered by the un-availability of routine and sufficiently precise measurements for the impurity concentration, c_z, in the highly radiating divertor region. In addition, the relation of momentum and volumetric power losses requires further investigations. Interesting and close correlations between the losses and the molecular density were found by Stangeby and Sang by a closer investigation of SOLPS 2D modelling results [47], but their explanation still remains to be identified. Molecular D_2 effects may turn out less important with a tungsten divertor compared e.g. to carbon, since the atomic D reflection rate is much higher on W [48].

The limit for the upstream separatrix density $n_{e,sep} \leq n_{GW}/2$ [11] is based on the critical ballooning α of a standard H-mode edge. Increased triangularity or edge profile tailoring may thus allow access to increased $n_{e,sep}$ values, and hence also to higher divertor pressure and radiation. Both the density-related radiation model and the flux related model suggest a high Greenwald density to allow for a high divertor radiation level. A high neutral pressure appears to be a key element for the exhaust of high power densities, therefore this parameter is suggested to be used as scaling parameter both in modelling and in experiment.

The inner divertor has not been considered here. It is for standard field direction (ion grad-B drift towards the X-point) in deeper detachment in comparison to the outer divertor and therefore less critical regarding power exhaust. Due to a stronger impact of the high field side high density region and other 2-D effects, the simple models used here are less applicable to the inner divertor.

Future work for improvement of the extrapolations should include experimental variations of machine size and power width, accompanying calculations with 2D codes like SOLPS for data validation and impurity enrichment,

improvement of atomic data for diagnostic spectroscopic lines, and turbulence studies on the divertor heat flux broadening.

Acknowledgement
This work has been carried out within the framework of the EUROfusion Consortium and has received funding from the Euratom research and training programme 2014-2018 under grant agreement number 633053. The views and opinions expressed herein do not necessarily reflect those of the European Commission.

[1] WENNINGER, R. et al., Nucl. Fusion **57** (2017) 016011.

[2] EICH, T. et al., Phys. Rev. Lett. **107** (2011) 215001.

[3] GALLO, A. et al., Plasma Phys. Controlled Fusion **60** (2018) 014007.

[4] LEONARD, A. W., Plasma Phys. Controlled Fusion **60** (2018) 044001.

[5] KALLENBACH, A. et al., Journal of Nuclear Materials **415** (2011) S19.

[6] STANGEBY, P., *The Plasma Boundary of Magnetic Fusion Devices*, Institute of Physics Publishing, Bristol and Philadelphia, 2000.

[7] KALLENBACH, A. et al., Plasma Physics and Controlled Fusion **60** (2018) 045006.

[8] KUKUSHKIN, A. S. et al., Nuclear Fusion **43** (2003) 716.

[9] KUKUSHKIN, A. et al., J. Nucl. Mater. **438** (2013) S203.

[10] GOLDSTON, R. et al., Plasma Phys. Controlled Fusion (2017) 055015.

[11] EICH, T. et al., Nuclear Fusion **58** (2018) 034001.

[12] BEURSKENS, M. et al., Nuclear Fusion **56** (2016) 056014.

[13] BERNERT, M. et al., Nuclear Materials and Energy **12** (2017) 111 , Proceedings of the 22nd International Conference on Plasma Surface Interactions 2016, 22nd PSI.

[14] KRASHENINNIKOV, S. and KUKUSHKIN, A., J. Plasma Phys. **83** (2017) 1.

[15] KALLENBACH, A. et al., Nuclear Fusion **52** (2012) 122003.

[16] BERNERT, M. et al., Review of Scientific Instruments **85** (2014) 033503.

[17] HENDERSON, S. S. et al., Nucl. Fusion **58** (2018) 016047.

[18] ADAS, www.adas.ac.uk/manual.php .

[19] POST, D. et al., Phys. Plasmas **2** (1995) 2328.

[20] SAMM, U. et al., Journal of Nuclear Materials **176-177** (1990) 273.

[21] KALLENBACH, A. et al., Plasma Physics and Controlled Fusion **58** (2016) 045013.

[22] DRENIK, A. et al., this conference, to be published in Nuclear Materials and Energy (2018).

[23] HENDERSON, S. et al., An assessment of nitrogen concentrations from spectroscopic measurements in the JET and ASDEX Upgrade divertor, this conference, to be published in Nuclear Materials and Energy (2018).

[24] ROHDE, V. et al., Physica Scripta **T138** (2009) 014024 (5pp).

[25] KALLENBACH, A. et al., Nuclear Fusion **55** (2015) 053026.

[26] POTZEL, S. et al., Journal of Nuclear Materials **463** (2015) 541.

[27] GOLDSTON, R., Nucl. Fusion **52** (2012) 013009.

[28] DUNNE, M. G. et al., Plasma Physics and Controlled Fusion **59** (2017) 025010.

[29] STEFANIKOVA, E. et al., Nucl. Fusion **58** (2018) 056010.

[30] MARTIN, Y. R. et al., Journal of Physics: Conference Series **123** (2008) 12033.

[31] PÜTTERICH, T. et al., Determination of the Tolerable Impurity Concentrations in a Fusion Reactor using a Consistent Set of Cooling Factors, submitted to NF (2018).

[32] BOSCH, H.-S. et al., Journal of Nuclear Materials **290–293** (2001) 836.

[33] LOARTE, A. et al., Nucl. Fusion **47** (2007) S203.

[34] KALLENBACH, A. et al., Nuclear Fusion **57** (2017) 102015.

[35] WADE, M. R. et al., J. Nucl. Mater. **266-269** (1999) 44.

[36] DUX, R. et al., Nuclear materials and Energy (2017).

[37] REIMOLD, F. et al., Nuclear Fusion **55** (2015) 033004.

[38] FIELD, A. et al., Plasma Phys. Controlled Fusion **59** (2017) 095003.

[39] LIPSCHULTZ, B. et al., Nucl. Fusion **56** (2016) 056007.

[40] LEONARD, A. et al., Nucl. Fusion **57** (2017) 086033.

[41] STANGEBY, P. C., Plasma Phys. Controlled Fusion **60** (2018) 044022.

[42] REIMOLD, F. et al., Comparing theoretical and experimental scalings for power exhaust in seeded H-modes with SOLPS simulations of ASDEX Upgrade, this conference, to be published in Nuclear Materials and Energy (2018).

[43] REINKE, M., Nucl. Fusion (2017) 034004.

[44] LOARTE, A. et al., Phys. Plasmas **18** (2011) 056105.

[45] ASAKURA, N. et al., Nucl. Fusion **57** (2017) 126050.

[46] SUBBA, F. et al., Plasma Phys. Controlled Fusion **60** (2018) 035013.

[47] STANGEBY, P. C. and SANG, C., Nucl. Fusion **57** (2017) 056007.

[48] BRIDA, D. et al., Nuclear Fusion **57** (2017) 116006.